Molecular Salts of Anesthetic Lidocaine with Dicarboxylic Acids: Solid-State Properties and a Combined Structural and Spectroscopic Study

Dario Braga;Laura Chelazzi;Fabrizia Grepioni;Elena Dichiarante;Michele R. Chierotti;Roberto Gobetto. Molecular Salts of Anesthetic Lidocaine with Dicarboxylic Acids: Solid-State Properties and a Combined Structural and Spectroscopic Study. CRYSTAL GROWTH & DESIGN. 13 pp: 2564-2572. DOI: 10.1021/cg400331h

CHARACTERIZATION OF FOUR MOLECULAR SALTS OF LIDOCAINE AND AN INVESTIGATION OF THEIR SOLID-STATE PROPERTIES

D. Braga,[a] E. Dichiarante,[b] F. Grepioni,[a] L. Chelazzi, M. R. Chierotti[c] and R. Gobetto[c]
[a] Ciamician
[b] PolyCrystalLine s.r.l., via F. S. Fabri 127/1, 40059 Medicina, Italy
[c] UniTO

Abstract

Four lidocaine molecular salts of dicarboxylic acids (oxalic, fumaric, malonic and succinic) were synthesized and characterized by different solid-state techniques: X-ray powder diffraction, Single Crystal – XRD; differential scanning calorimetry, FT-IR and solid-state NMR (^{1}H MAS and CRAMPS, and ^{13}C and ^{15}N CPMAS). The structure of the hydrogen succinate salt was determined from powder diffraction data with the support of information obtained by ^{1}H DQ CRAMPS and ^{1}H-^{13}C off-resonance FSLG HETCOR solid-state NMR experiments. All molecular salts show a dramatic increase in their melting point with respect to both lidocaine and lidocaine hydrochloride, while both solubility and dissolution rate in water are higher with respect to the free base, though lower than those observed for the chloride salt.

Introduction

The preparation of multi-component molecular crystals is at the forefront of crystal engineering studies. The goal is that of being able to device new "collective" properties by binding together within a same crystal structure an active molecule, e.g. an active pharmaceutical ingredient (API), and one or more partner molecules, whether active or "innocent", in order to obtain new and improved crystal properties with respect to those of the original solid. The hydrogen bond is the interaction of choice in the making of co-crystals because it combines, strength, directionality and, at least to a considerable extent, predictability. For these reason many co-crystals are obtained by combining and acidic molecule and a base, linked together via hydrogen bonds. However, it is not always possible to predict the outcome of the reaction, i.e. whether the proton will remain bound to the donor group (often a –COOH) or will be transferred to the acceptor base or will adopt some intermediate location along the D---H---O vector. X-ray diffraction often gives an ambiguous

answer, and only spectroscopic techniques allow to understand if the multi-component crystal is a co-crystal or a molecular salt.

In this study we address this issue by investigating cooperatively, by single crystal and powder diffraction X-ray and ^{13}C and ^{15}N solid state NMR spectroscopy, the case of the interaction between lidocaine and four organic salts, namely oxalic, fumaric, malonic and succinic acid. Solid state properties of the resulting products are also addressed.

Lidocaine (2-diethylamino-N-(2,6-dimethylphenyl)acetamide) is an amide-type anesthetic molecule, firstly synthesized by Nils Löfgren in 1943.[1] Lidocaine (Scheme 1 for both neutral and protonated forms) is a typical local anesthetic, also used for the treatment of ventricular tachycardia (a cardiac arrhythmia) as intravenous injection solution (See e.g. U.S. Patent No. 3,968,205).

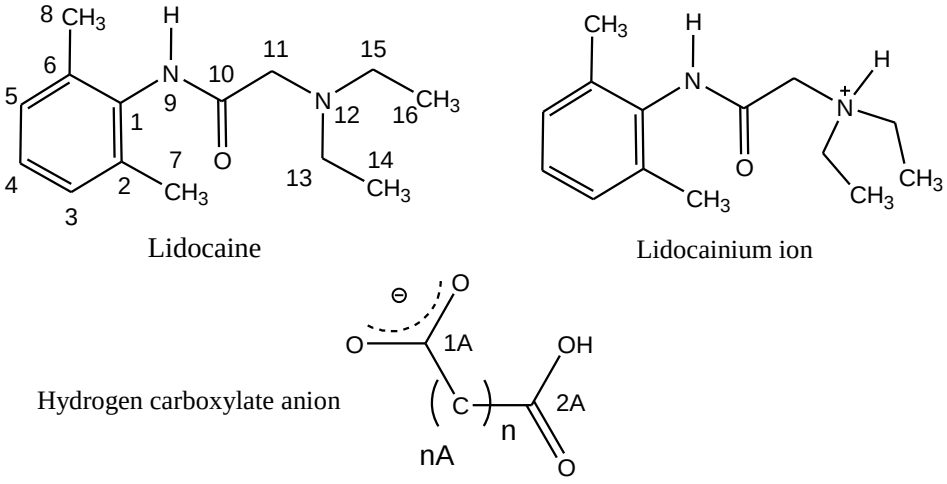

Scheme 1.

Lidocaine is also widely used as a vasoconstrictor to reduce regional blood flow in topical applications or aerosols (such as nasal aerosols to reduce nasal congestion: See U.S. Pat. No. 5,534,242). In addition to this, it is known for its therapeutic effects in reducing post-herpetic neuralgia (PHN), nerve injury pain from shingles (herpes zoster and post herpetic neuralgia) and analogous neuropathies. For example, U.S. Pat. No. RE37,727 discloses methods employing lidocaine intradermal administration by transport of lidocaine from the skin surface, using patches and dressings, into the skin.[2]

Lidocaine is present in the European Pharmacopoeia in two forms: the free base, not very stable and characterized by a very low solubility in aqueous solution, and the chloride salt, characterized by a

very high solubility in aqueous solution and used generally for the preparation of injection solutions.

To modify and improve solubility, stability and therefore efficacy of the free base, lidocaine is usually made available as salts. In the literature several examples are reported of lidocaine salts with organic acids, studied to improve the properties of the free base and with other active ingredients to combine different therapeutic effects in the same drug,[3] but no structural characterization is available.

Lidocaine in both its neutral and cationic forms is represented in Scheme 1 together with the labeling scheme.

In the present study four molecular salts of lidocaine with oxalic, malonic, succinic and fumaric acid were prepared using both conventional solution chemistry and mechanochemical methods by mixing of reactants in the solid phase (grinding or kneading).[4] Table 1 lists the molecular salts prepared, together with their labeling scheme.

Table1. Molecular salts resulting from the reaction of lidocaine with the dicarboxylic acids.

acid	**molecular salt**
oxalic HOOC-COOH	[lidocainium][Hoxalate] **1H hydrogen oxalate**
malonic $HOOC(CH_2)COOH$	[lidocainium][Hmalonate] **1H hydrogen malonate**
succinic $HOOC(CH_2)_2COOH$	[lidocainium][Hsuccinate] **1H hydrogen fumarate**
fumaric $HOOC(CH)_2COOH$	[lidocainium][Hfumarate] **1H hydrogen succinate**

All solid products were characterized by X-ray powder diffraction (XRPD), differential scanning calorimetry (DSC), and FT-IR. Further insights on salt or co-crystal nature[5] and hydrogen bond (HB) interactions[6] of the samples were obtained by means of 1D (^{1}H MAS and CRAMPS, ^{13}C and ^{15}N CPMAS) and 2D (^{1}H double-quantum, DQ, CRAMPS and ^{1}H-^{13}C on- and off-resonance FSLG HETCOR) solid-state NMR (SS NMR) experiments. The lidocaine hydrogen oxalate, hydrogen fumarate and hydrogen malonate salts were also characterized by single crystal X-ray diffraction (SC-XRD). The structure of lidocainium hydrogen succinate (**1H hydrogen oxalate**) was determined from X-ray powder diffraction assisted by SS NMR data, which provided information on the number of independent molecules, HB network and crystal packing through the analysis of ^{1}H-^{1}H or ^{1}H-^{13}C proximities.[7]

In addition to the synthesis and solid-state characterization, the salts were also subjected to dissolution tests in aqueous solution and the results were compared with thermodynamic and kinetic solubility of lidocaine and lidocaine hydrochloride.

Experimental section

All reactants were purchased from Aldrich and used without further purification. Reagent grade solvents and doubly-distilled water were used. For dissolution tests a 0.9%. sodium chloride solution was used.

Solution synthesis

All salts were crystallized by room temperature evaporation of a solution obtained dissolving a stoichiometric mixture (1:1) of lidocaine and organic acid in hot methanol 99.8%. The amount of reagent was chosen so that 200-300mg of solid product could be obtained.

Mechanochemistry

All salts were quantitatively obtained as polycrystalline materials by grinding or kneading (grinding in the presence of a small quantity of water)[4] of lidocaine and organic acid in a 1:1 stoichiometric ratio. The experiments were performed with a Retsch MM 200 grinder for 15 minutes at a frequency of 30Hz.

Thermal measurements

Calorimetric measurements were performed using a DSC 200 *F3 Maia*® differential scanning calorimeter equipped with an intra-cooler. The samples (2–4 mg) were placed in pierced aluminium pans, and the heating was carried out at 10°C min^{-1} in N_2 atmosphere (see ESI).

Single crystal X-ray diffraction

Single-crystal data were collected on an Oxford X'Calibur S CCD diffractometer equipped with a graphite monochromator (MoKα radiation, λ = 0.71073) and operated at room temperature. The structure was solved by direct methods and refined by full-matrix least-squares on F^2 with the SHELX97[8a] program package.

A calculated XRPD pattern was generated via Mercury[8b] v 1.4 on the basis of single crystal data. Mercury and SCHAKAL99[8c] were used for the graphical representation of the results and PLATON[8d] was used for hydrogen bonding analysis.

Powder X-ray diffraction

Diffraction patterns from 3° to 40° in 2θ were collected on a PANalytical diffractometer with Bragg–Brentano geometry (Cu Kα radiation, detector X'celerator, step size Δ2θ = 0.0167°, counting time per step = 20 s), using a glass sample holder. The tube voltage and amperage were set to 40 kV and 40 mA, respectively.

For the structure solution of **1H hydrogen succinate** from X-ray powder diffraction a diffraction pattern was collected from 5 to 70° in 2θ with a step size of 0.00835° and counting time per step = 50 s. The structure was solved by analogy with the structure of **1H hydrogen fumarate**, and refined by Rietveld analysis. Rietveld refinement was performed with the software GSAS.[9]
A cosine Fourier series with 10 coefficients and a pseudo-Voigt function (type 3) were used to fit respectively background and peak shape. A spherical harmonics model was used to describe preferred orientation. Soft constraints were applied on bond distances and angles of both molecules. An overall thermal parameter for each atom species was adopted. Refinement converged with χ^2 = 11.04, R_{wp} = 10.84 R_{F2}= 8.96. Figure 1 shows experimental, calculated and difference curves.

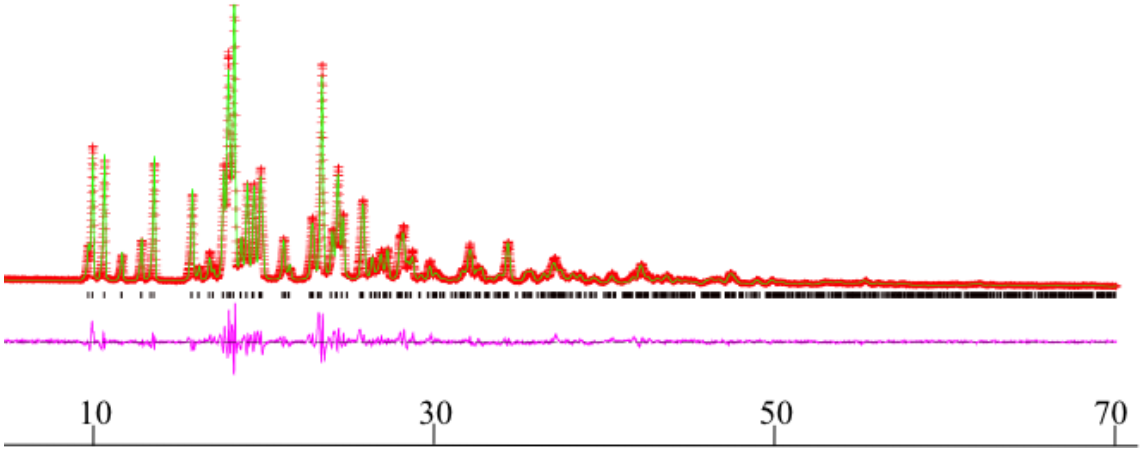

Figure 1. Experimental (red crosses), calculated (green) and difference (purple) curves for crystalline **1H hydrogen succinate**.

FT-IR

All FT-IR measurements were performed using a Nicolet FT-IR 6700 Thermo Fischer equipped with ATR device. The analyses were performed on all samples and for each measurement 32 scans were performed (see ESI).

SSNMR spectroscopy

SSNMR measurements were run on a Bruker AVANCE II 400 instrument operating at 400.23, 100.65 and 40.55 MHz for ^{1}H, ^{13}C and ^{15}N, respectively. ^{13}C, ^{15}N and 2D HETCOR spectra were recorded at room temperature at the spinning speed of 12 (^{13}C and 2D) or 7 kHz (^{15}N). Cylindrical 4mm o.d. zirconia rotors with sample volume of 80 µL were employed. For ^{13}C and ^{15}N CPMAS experiments, a ramp cross-polarization pulse sequence was used with contact times of 4 ms, a ^{1}H 90° pulse of 3.30 µs, recycle delays of 2-6 s, and 124 (^{13}C) or 256-1024 (^{15}N) transients. The two

pulse phase modulation (TPPM) decoupling scheme was used with a frequency field of 75 kHz. Spectral editing experiments were performed by using a CPPISPI pulse sequence with a polarization inversion time of 65-85us in order to obtain CH_3 and C_q positive, CH null and CH_2 negative (Figure S11 in the supplementary material). 2D ^1H-^{13}C on- and off-resonance HETCOR spectra were measured according to the method of van Rossum et al.[10] with setup previously described.[11] The ^1H chemical shift scale in the HETCOR spectra was corrected by a scaling factor of $1/\sqrt{3}$ since the ^1H chemical-shift dispersion is scaled by a factor of $1/\sqrt{3}$ during FSLG decoupling. ^1H MAS, ^1H CRAMPS and 2D ^1H DQ CRAMPS experiments were performed on a 2.5 mm Bruker probe. The ^1H MAS spectra were acquired at the spinning speed of 32 kHz with the DEPTH sequence ($\pi/2$–π–π) for the suppression of the probe background signal. ^1H CRAMPS spectra were acquired using a windowed-PMLG5 (*w*-PMLG5)[12a] pulse sequence of dipolar decoupling at the spinning speed of 12.5 kHz. 2D ^1H DQ CRAMPS spectra were acquired at the spinning speed of 12.5 kHz with PMLG5 and *w*-PMLG5 pulse sequences for homonuclear dipolar decoupling during t_1 and t_2, respectively. For all samples, ^1H 90° pulse lengths of 2.5 μs and recycle delays of 3 s were used. For each of 256 increments of t_1, 80 transients were averaged. The pulse width and the RF power were finely adjusted for best resolution. In t_2, one complex data point was acquired in each acquisition window (2.2 μs). DQ excitation and reconversion was achieved using three elements of POST-C7,[12b] corresponding to a recoupling time of 68.58 μs. A 16-step nested phase cycle was used to select Dp=±2 on the DQ excitation pulses (four steps), and Dp=-1 on the z-filter 90° pulse (four steps). The States-TPPI method was used to achieve sign discrimination in the F1 dimension.

^1H, ^{13}C and ^{15}N scales were calibrated with adamantane (^1H signal at 1.87 ppm), glycine (^{13}C methylene signal at 43.86 ppm) and $(NH_4)_2SO_4$ (^{15}N signal at δ=355.8 ppm with respect to CH_3NO_2) as external standards.

Dissolution tests

The calibration curve was constructed by plotting the values of absorbance against those of concentrations for four standard solutions of the sample in a sodium chloride solution 0.9% in standard concentrations. The analyses were performed using a dissolution tester and methods as described in the "*European Pharmacopeia section 2.9.3 pg. 267"*. The program used was "*Concentration*" (Cary 50 WinUV Software V.3) and the measurement for each standard was recorded at a fixed λ. The dissolution rates were performed on a Hanson's Vision Classic 6 dissolution tester coupled with a Varian Cary 50 UV-Vis Spectrophotometer. The program used was "*Kinetic"* (Cary 50 WinUV Software V.3), which recorded continuously the absorbance at

fixed λ of a sodium chloride solution 0.9% (80mL) under stirring (250rpm) at 37°C in which were added approximately 10mg of sample. The values obtained were converted from Abs/min to mol/min and for each sample two measurements were recorded. The thermodynamic solubilities were measured by leaving a sodium chloride solution 0.9% of the sample under stirring at 500 rpm for 24 h at 37°C. Then the suspensions were filtered, diluted and analyzed by UV-Vis Cary 50 Varian equipped with an optic fiber. Results were obtained using the calibration curves built in the first part of the experiment. For each sample two measurements were taken (see ESI for details).

Results and discussion

Four molecular salts of lidocaine were synthesized by reaction with carboxylic acids: lidocainium hydrogen oxalate (**1H hydrogen oxalate**), lidocainium hydrogen malonate (**1H hydrogen malonate**), lidocainium hydrogen succinate (**1H hydrogen succinate**) and lidocainium hydrogen fumarate (**1H hydrogen fumarate**); they were crystallized by evaporation at room temperature from methanol solution or obtained by grinding or kneading. The four salts were investigated by solid-state techniques such as X-ray powder diffraction, differential scanning calorimetry, FT-IR and SS NMR. Solid **1H hydrogen oxalate**, **1H hydrogen malonate** and **1H hydrogen fumarate** were also characterized by SC-XRD. In these three cases correspondence between the structure determined by SC-XRD and the bulk material was checked by comparing calculated and measured diffraction patterns (See supplementary material).

In the structure of **1H hydrogen oxalate** two hydrogen bonds [O(H)···O 2.723(2)Å] connect the hydrogen oxalate anions, which form dimers. These "lateral" dimers, based on 10 atom rings, are not frequently found, as the majority of hydrogen bonded dimers involving hydrogen oxalates is based on 8 atom rings (see Scheme 2). The motif has been found by us and other authors in only eight organic/organometallic molecular salts (CSD refcodes AHESIP, AHESOV, BOTKUR, KITKII, QIGCIS, YEPBAX, EZECOC, PAXKAC), in which the O(H)···O distances within the dimer range from 2.581 to 2.721Å. The carboxylate group of the hydrogen oxalate anion is bound to two lidocainium cations through two hydrogen bonds HBs, one with the amido group and the other with the amino group (see Fig. 2a). The hydrogen oxalate dimers bridge lidocainium cations forming chains. The main packing pattern in crystalline **1H hydrogen oxalate** can thus be seen as constituted of hydrogen bonded chains arranged in layers (see Figure 3a).

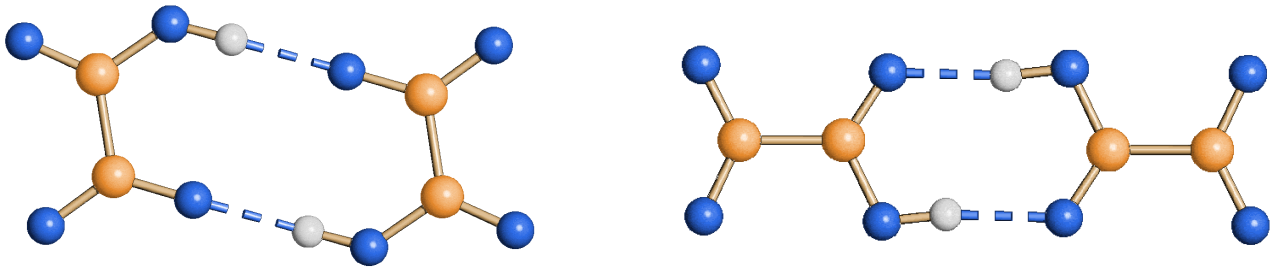

Scheme 2. "Lateral" hydrogen bonded dimer (left) formed by hydrogen oxalate anions in lidocainium hydrogen oxalate, **1H hydrogen oxalate** [O(H)···O 2.723(2)Å]. The more common hydrogen bonded ring is shown on the right.

In crystalline **1H hydrogen malonate** the hydrogen malonate anions act as bridges between lidocainium cations. The malonate anion forms one intramolecular [O(H)···O 2.460(9) and 2.380(9)] Å and an intermolecular hydrogen bond with the amido group of the lidocainium cation [N(H)···O 2.880(6) and 2.837(6)Å] (see Figures 2b and 3b).

The structure of **1H hydrogen succinate** was determined from X-ray powder diffraction data, using also the analogy with the structure of **1H hydrogen fumarate**, and was refined by Rietveld analysis.

In crystalline **1H hydrogen succinate** the carboxylate group forms hydrogen bonds with the amido group of one lidocainium cation (see Figure 2c), resulting in an infinite chain (Figure 3c).

Crystalline of **1H hydrogen fumarate** is isomorpous with crystalline **1H hydrogen succinate**, as it can be seen from Figures 2d and 3d, which show the same arrangement of hydrogen bonding interactions and packing features [N(H)···O_{amido} 2.821(5) Å, N(H)···O_{amino} 2.882(6) Å, $O(H)_{anion}$···O_{anion} 2.537(6) Å] .

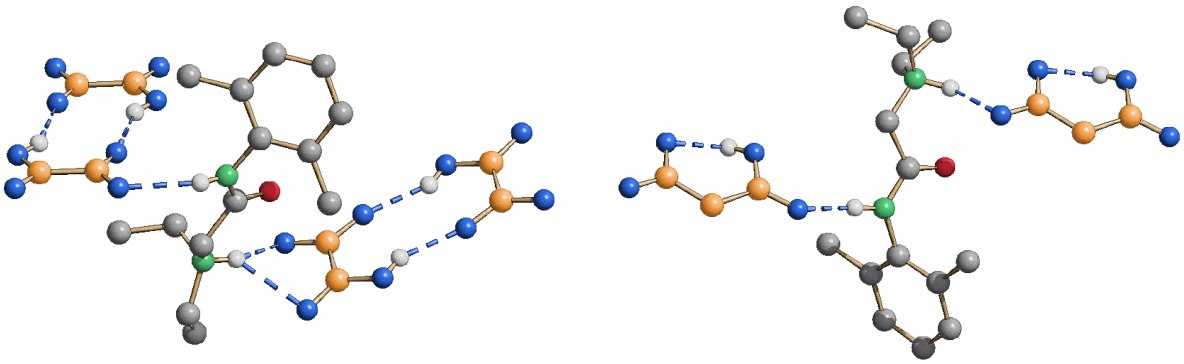

(a) (b)

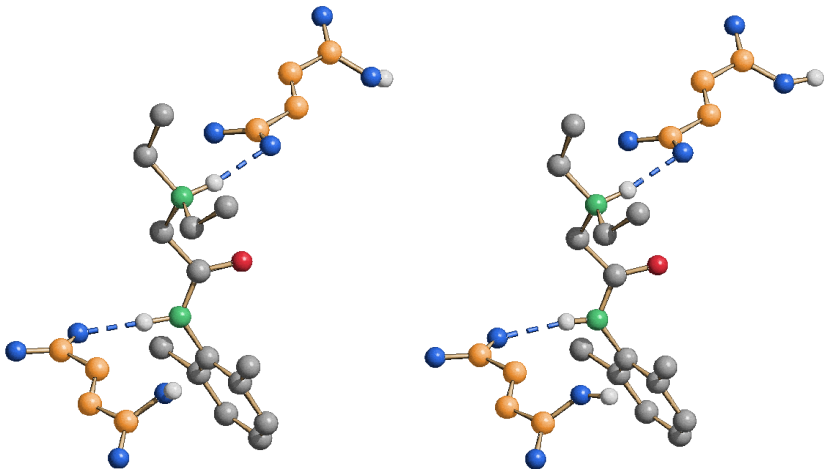

(c) (d)

Figure 2. Relevant hydrogen bonding interactions between the lidocainium ion and the (a) hydrogen oxalate, (b) hydrogen malonate, (c) hydrogen succinate and (d) hydrogen fumarate anions in their respective **1H** molecular salts.

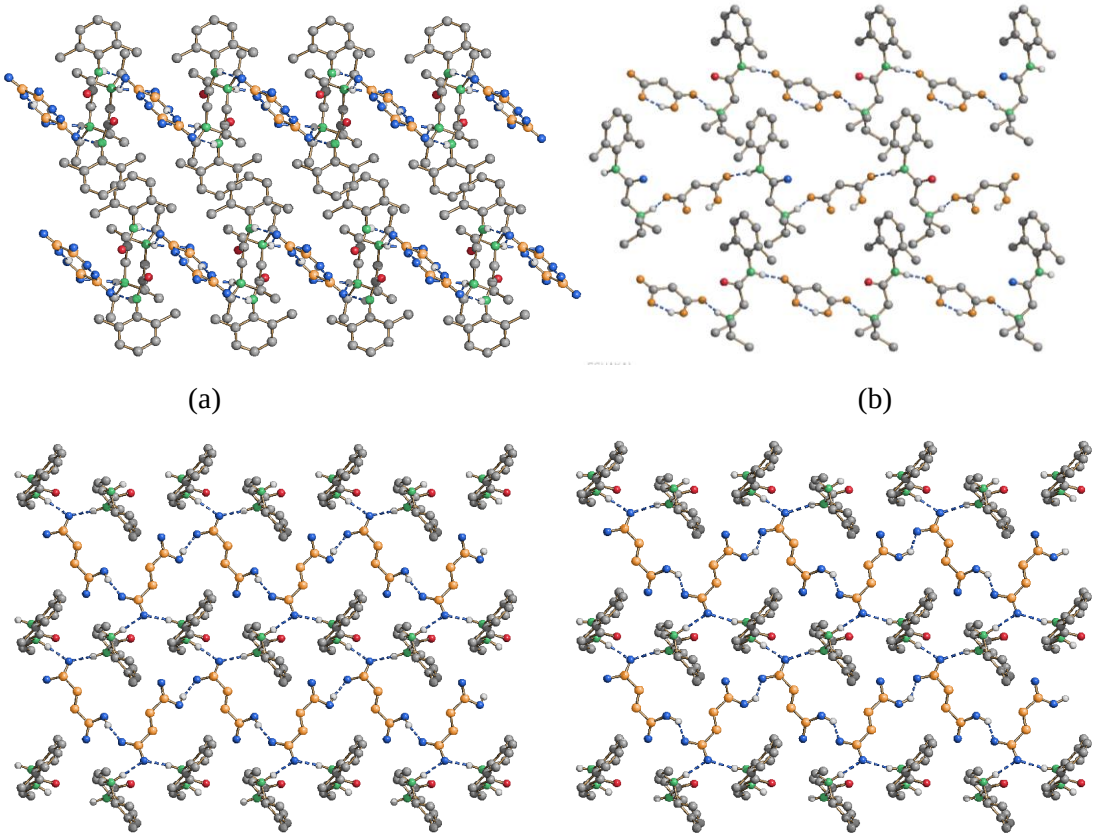

(a) (b)

(c) (d)

Figure 3. Hydrogen bonding patterns in solid **1H hydrogen oxalate** (a), **1H hydrogen malonate** (b), **1H hydrogen succinate** (c) and **1H hydrogen fumarate** (d).

Table 2. Crystal data and measurement details for compounds **1H hydrogen oxalate**, **2**, **3** and **4.**

	1H hydrogen oxalate	**1H hydrogen malonate**	**1H hydrogen succinate**	**1H hydrogen fumarate**
Formula	$C_{16}H_{24}N_2O_5$	$C_{17}H_{23}N_2O_5$	$C_{18}H_{28}N_2O_5$	$C_{18}H_{26}N_2O_5$
M_r	324.37	336.38	352.43	350.41
System	Monoclinic	Triclinic	Orthorombic	Orthorombic
space group	$P2_1/c$	P-1	$P2_12_12_1$	$P2_12_12_1$
a [Å]	10.5817(8)	10.486(4)	10.4949(3)	10.442(5)
b [Å]	10.3447(5)	10.302(3)	10.8924(3)	10.962(5)
c [Å]	15.3496(1)	12.302(4)	16.581(4)	16.273(5)
α [°]	90.00	74.81(4)	90.00	90.00
β [°]	102.719(7)	87.50(5)	90.00	90.00
γ[°]	90.00	89.97(5)	90.00	90.00
V [Å³]	1639.01(18)	1920.7(9)	1895.4(6)	1862.7(14)
Z	4	4	4	4
d_{calc}	1.315	1.170	-	1.250
F(000)	696	728	-	752
measured reflns	7219	9367	-	5838
unique reflns	3744	6878	-	3974
refined parameters	226	433	-	238
GOF on F²	1.032	1.063	-	1.027
R1 [on F, I>2σ(I)]	0.0784	0.0898	-	0.0869
wR2(onF²,all data)	0.2002	0.3620	-	0.1941

The SSNMR technique has been helpful to the definition of the crystal nature, in particular in addressing the question about whether the compounds discussed herein ought to be regarded as neutral molecular co-crystals or as ionic molecular salts. The difference is subtle depending on whether the proton along the O-H···N interaction remains close to oxygen or moves close to nitrogen. Moreover, proton transfer from the acid to the base, beside depending on the relative values of pK_a (but beware of the fact that pK_a is evaluated with respect to the solvent, usually water, and not in the solid state)[13a] it also depends on the temperature. There are several examples in the literature[13b] where the position of the proton is shown to move along the D---H---A vector. In these cases the use of NMR spectroscopic methods, such as the measurement of ^{13}C chemical shifts of carboxylic carbon atoms represent good indicators of the protonated state of COOH groups.[14a-c] Furthermore, ^{15}N NMR studies have shown that protonation or formation of HBs result in a shift of the nitrogen signal at high- or low-frequency, according to the type of nitrogen atom and the interaction nature.[14d–f,15]

Table 3 lists ^{1}H, ^{13}C and ^{15}N chemical shifts of the groups involved in HBs only, while all chemical shifts with assignments (done by combining 2D and spectral editing experiments) are reported in supplementary material (Table S1) together with an additional analysis of the ^{13}C and 2D spectra. For atom labeling see Scheme 1.

The analysis of the ^{13}C resonances around 160-179 ppm and of the ^{15}N signal around 14-29 ppm allowed to ascertain the transfer of a single proton from the acid to lidocaine with formation of one carboxylate and one ammonium group. Accordingly, all adducts can be described as molecular salts. Indeed, the ^{13}C spectra (Figure S1) are characterized by a signal at high frequencies (166-169 ppm) typical of carboxylate carbon atoms together with a peak around 162-166 ppm attributed to COOH. In the ^{15}N CPMAS spectra (Figure S2) the shift amplitude of the N12 signal (from 15-17 ppm in lidocaine to about 25-29 ppm in the salts) indicates the complete protonation of the nitrogen atom in agreement with the ionic nature detected by X-ray diffraction and ^{13}C CPMAS spectra.
On the other hand, ^{1}H CRAMPS spectra (whose improved resolution is compared to MAS spectra in Figure 4) allowed the characterization of the hydrogen bonds in term of their presence and strenght, the latter depending on the high-frequency shift extent of the signals attributed to hydrogen-bonded protons.[16] The ^{1}H chemical shift values for hydrogen-bonded protons are reported in Table 3 for all values (see Table 2S in the supplementary material).
The strongest hydrogen bonds are those associated to O···H···O interactions between acid molecules with ^{1}H chemical shift around 12.5-15 ppm. In particular, the ^{1}H CRAMPS spectrum of **1H hydrogen malonate** (Figure 4c) is characterized by a resonance typical of a very strong HB at 19.5 ppm, attributed to H1A which is involved in the intramolecular O···H···O interaction, similar to that previously observed in the malonic acid:dabco co-crystal.[17] The N-H···O contacts are weaker with ^{1}H chemical shifts around 10-11.6 ppm, while the $^{+}$N-H···O^{-} interactions are the weakest as confirmed by their low chemical shift values (10.4, 9.3, 8.6 and 11.4 ppm) and large heavy atom distances (2.882 Å, 2.914 Å, 2.957 Å and 2.874 Å for the fumarate, malonate, oxalate and succinate salts, respectively).
SSNMR data were also useful in assisting and simplifying the structure solution from X-ray powder data of compound **1H hydrogen succinate**. The ^{13}C CPMAS spectrum assigns Z' = 1 for both lidocaine and the acid molecule. The similarity of crystal packing and HB networks between fumarate and succinate salts is confirmed by the analysis of ^{1}H-^{1}H or ^{1}H-^{13}C proximities observed in their ^{1}H-^{13}C FSLG off-resonance HETCOR (Figure 5) and 2D ^{1}H DQ CRAMPS (Figures 6 and 7) spectra.
Common ^{1}H-^{13}C correlations, refering only to intermolecular proximities, can be resumed as follow and are depicted in Figure 5c: H1A correlates with C2A (δ^{1H}-δ^{13C}= 15.1-173.2 fumarate salt; 14.4-178.2 succinate salt) in agreement with the presence of chains of acid molecules linked by O-H···O interactions; H12 (δ = 10.4 and 11.4 ppm for fumarate and succinate salt, respectively) transfers polarization to C2A (δ = 173.2 ppm fumarate salt; 178.2 ppm succinate salt) confirming the presence of $^{+}$N-H···O^{-} HBs; H4 and H3 correlate with C1A and C2A, respectively (δ^{1H}-δ^{13C}= 6.3-

167.8 and 7.0-173.2 fumarate salt; 7.2-173.4 and 7.8-178.2 succinate salt) indicating the proximity between the aromatic ring and the acid; we also observe polarization transfer from H13 (or H15) to C3 and/or C4 since in both 3D structures they point towards the aromatic ring.

In the same way, other spatial information can be obtained by looking at the DQ signals (indicating ^{1}H-^{1}H proximities) in the 2D ^{1}H DQ CRAMPS spectra (Figures 6 and 7). Here we focus our attention only on ^{1}H-^{1}H intermolecular proximities characterizing molecular packing and HB environments while the complete list of DQ frequencies with assignment is reported in Table S3 (see Supplementary Material). Key comparison elements are DQ coherences between H3 and H1A, H3A and H4A (δ_{DQ}=7.8+14.4=22.2 ppm, δ_{DQ}=7.8+2.0=9.8 ppm, and δ_{DQ}=7.8+2.0=9.8 ppm, respectively) in the ^{1}H DQ CRAMPS spectrum of **1H hydrogen succinate** (Figure 6) indicating the proximity between the aromatic ring and the acid. Indeed, similar correlations have been found also in the spectrum of **1H hydrogen fumarate** (Figure 7) with DQ signals between H3-OH (δ_{DQ}=7.0+15.1=22.0 ppm) and H3-H4A (δ_{DQ}=7.0+6.3=13.3 ppm). Concerning the hydrogen bond environment, apart from the already mentioned H1A-H3 proximity, in both spectra H1A-H7 (δ_{DQ}=15.1+2.2=17.3 ppm for the fumarate salt; δ_{DQ}=14.4+1.8=16.2 ppm for the succinate salt) and H1A-H3A (δ_{DQ}=15.1+6.3=21.4 ppm for the fumarate salt; δ_{DQ}=14.4+1.8=16.2 ppm for the succinate salt) correlations are observed. All these elements contribute to confirm and validate the structure of **1H hydrogen succinate** solved from XRPD.

Table 3: ^{1}H, ^{13}C and ^{15}N chemical shifts with assignment of groups involved in HBs only for lidocaine, **1H hydrogen oxalate**, **1H hydrogen malonate**, **1H hydrogen succinate** and **1H hydrogen fumarate**.

atom	Note	lidocaine	1H hydrogen oxalate	1H hydrogen malonate	1H hydrogen succinate	1H hydrogen fumarate
C1A	COOH		162.7	174.9	173.4	167,8
C2A	COO^{-}		166.0	174.9	178.2	173,2
N9	NH	98.7	25.9	27.5	28.4	29.0
N12	N or NH^{+}	14.9 and 16.9	98.7	97.4	107.3	106.0
H1A	COOH		12.5	19.5	14,2	15.1
H9	NH	10.1 and 10.3	10.0	10.0	11.6	11.4
H12	NH^{+}		8.6	9.3	11.4	10.4

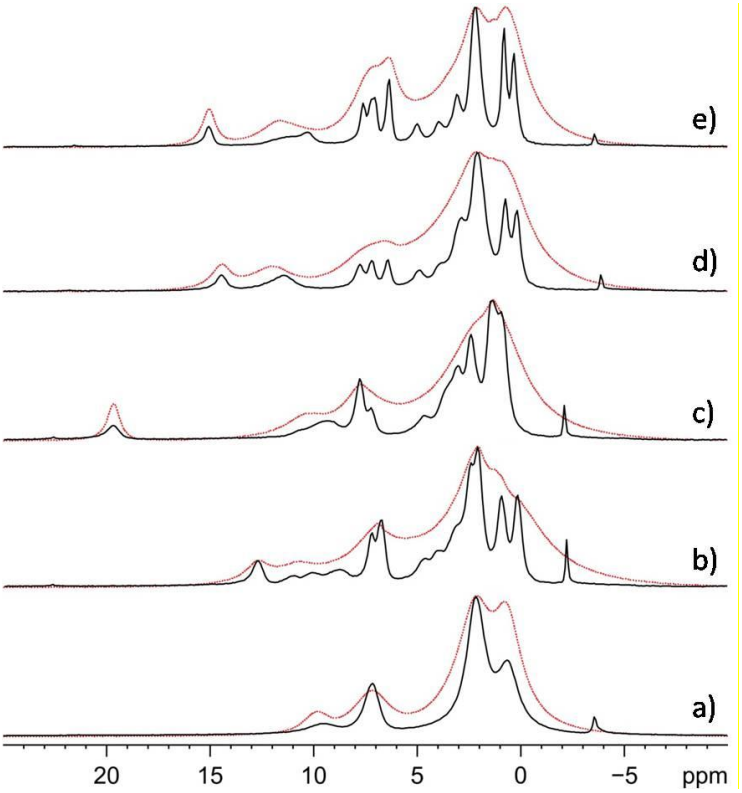

Figure 4. Comparison between ^{1}H (400.23 MHz) CRAMPS (black lines) and MAS (red dotted lines) spectra of lidocaine (a), **1H hydrogen oxalate** (b), **1H hydrogen malonate** (c), **1H hydrogen succinate** (d) and **1H hydrogen fumarate** (e) recorded with a spinning speed of 32 kHz.

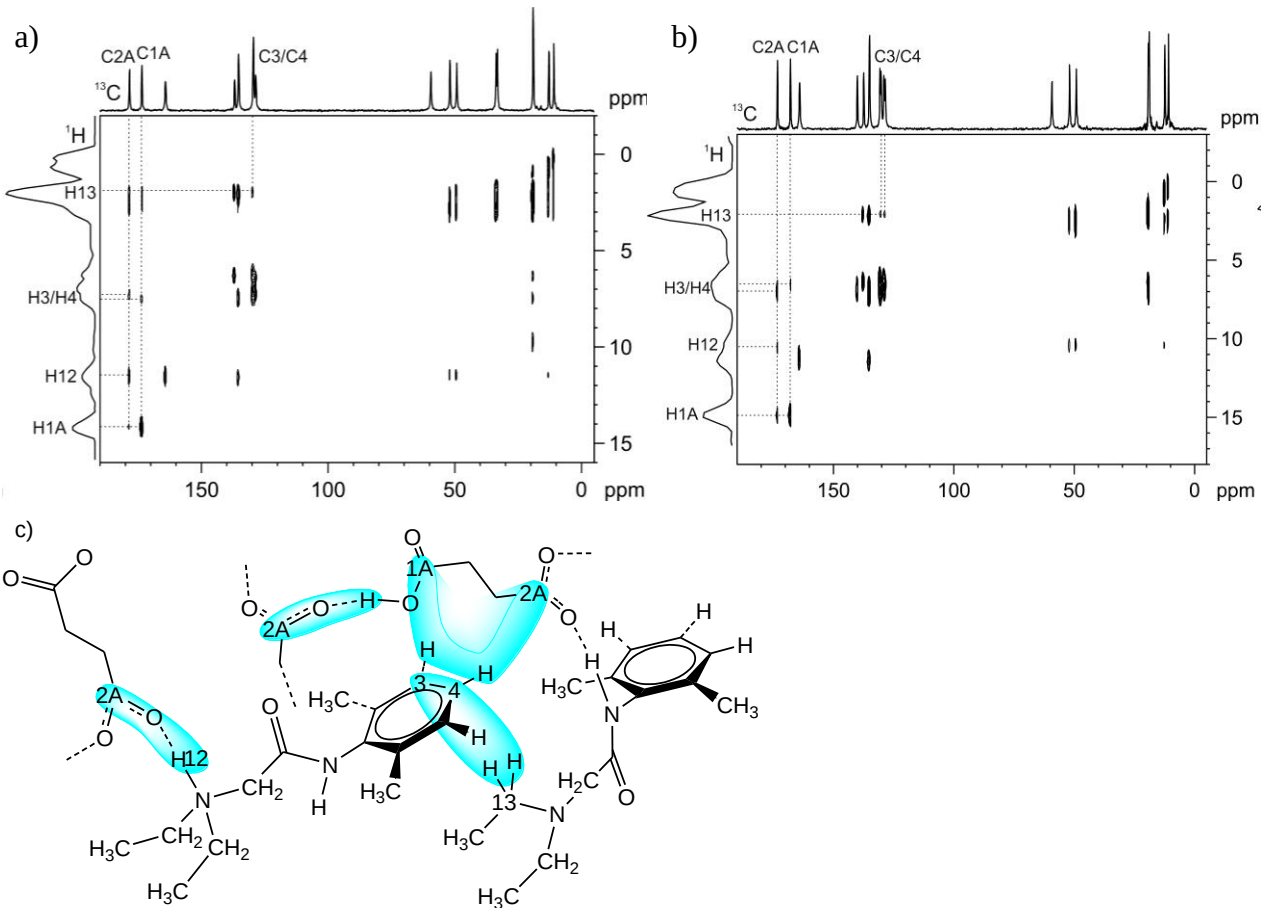

Figure 5. ^{1}H-^{13}C FSLG off-resonance HETCOR spectra of **1H hydrogen fumarate** (a) and **1H hydrogen succinate** (b) recorded with a contact time of 2 ms and a spinning speed of 12 kHz. (c) Representation of the crystal structure of **1H hydrogen fumarate** and **1H hydrogen succinate** showing the main ^{1}H-^{13}C intermolecular proximities characterizing the crystal packing of both salts (see discussion in the text).

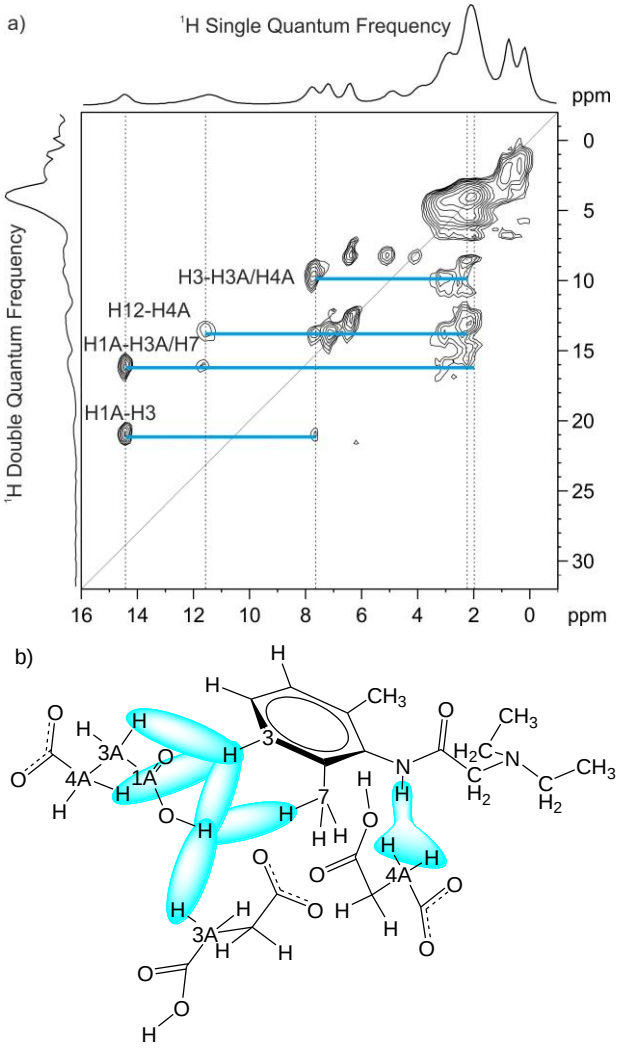

Figure 6. a) 2D ^{1}H-^{1}H DQ CRAMPS of **1H hydrogen succinate** recorded with a spinning speed of 12.5 kHz. Solid blue orizontal bars indicate specific DQ coherences among H1A, H3, H12, H3A and H4A. b) Representation of the crystal structure of **1H hydrogen succinate** showing the main ^{1}H-^{1}H intermolecular proximities characterizing crystal packing and HB enviroments (see discussion in the text).

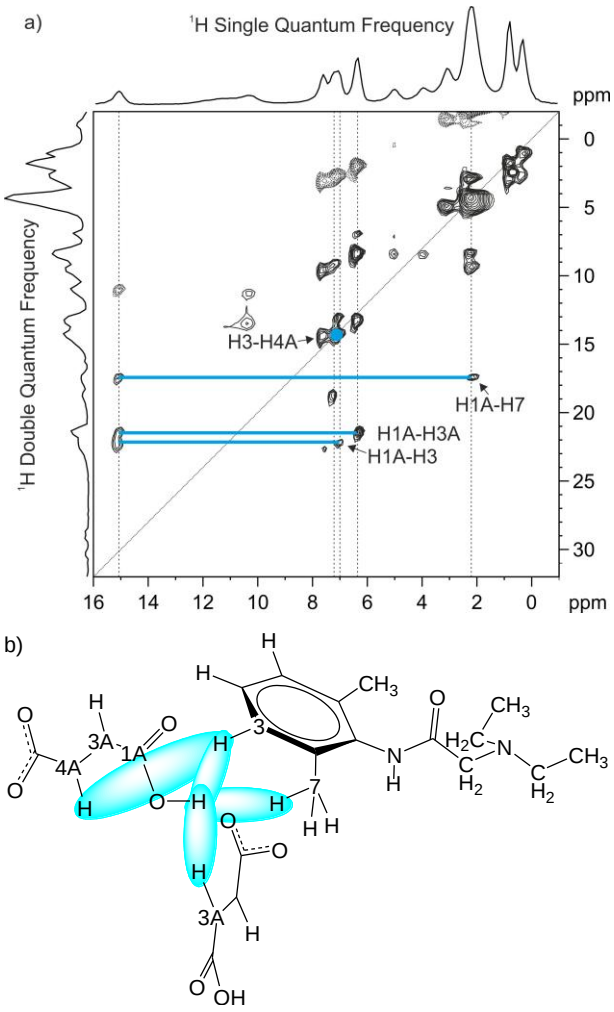

Figure 7. a) 2D ^{1}H-^{1}H DQ CRAMPS of **1H hydrogen fumarate** recorded with a spinning speed of 12.5 kHz. Solid blue orizontal bars indicate specific DQ coherences among H1A, H3, H3A and H4A. b) Representation of the crystal structure of **1H hydrogen fumarate** showing the main ^{1}H-^{1}H intermolecular proximities characterizing crystal packing and HB enviroments (see discussion in the text).

Differential scanning calorimetry was used to measure the melting point of all compounds and to detect the presence of additional crystalline phases.

As mentioned above, the salts have been also subjected to dissolution tests in aqueous solution and the results have been compared with thermodynamic and kinetic solubility of lidocaine free base and lidocaine hydrochloride salt.

In Table 4 the melting points and dissolution results of four carboxylic salts, hydrochloride salt and lidocaine free base are reported.

The results show an increase of the melting points on passing from the free base to the lidocaine carboxylic salts, in fact, the lidocaine free base and the hydrochloride salt reveal a melting point between 60°C and 70°C, while the salts synthesized present a melting point higher than 100°C.

The hydrogen malonate salt has been previously reported [3e] together with other salts of lidocaine (maleate, adipate and tosylate) and characterized by ^{1}H NMR, IR, MS, UV-Vis. Melting point, tests of skin permeability and apparent partition coefficients were also measured. The melting points of these salts, as that of samples characterized in the present work, have higher melting point than lidocaine and lidocaine hydrochloride.[3e]

The dissolution rates of lidocaine free base and hydrogen fumarate salt are lower than hydrogen succinate, hydrogen oxalate and hydrogen malonate salts, on the other hand these last three salts reveal a good thermodynamic solubility value exceeding 120 g/L.

The best value of dissolution rate is shown by the chloride salt, it also has the higher thermodynamic solubility. The results of kinetic solubilities are reported in Figure 8, where a comparison between the dissolution curves (ABS/min) is presented.

Table 4

Sample	mp(°C)	Thermodynamic Solubility (g/L)	Dissolution rate (mol/min)
1	67.5	3.13	$2.13*10^{-5}$
1 HCl	75.8	>633	$1.85*10^{-3}$
1H hydrogen oxalate	159.2	128.5	$1.05*10^{-4}$
1H hydrogen malonate	140.2	>279	$1.5*10^{-4}$
1H hydrogen succinate	113.5	>321	$1.5*10^{-4}$
1H hydrogen fumarate	186.9	71	$7.31*10^{-5}$

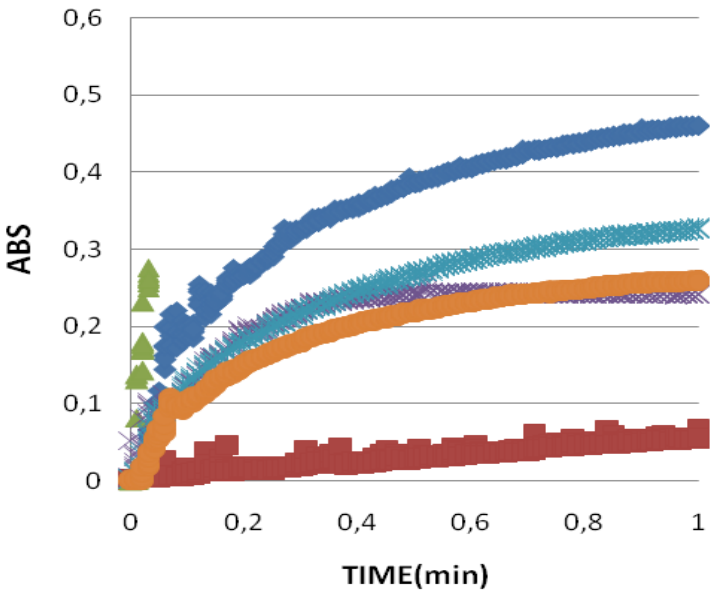

Figure 8: Dissolution profile.(red line: **1**; orange line: **1H hydrogen oxalate**; purple line: **1H hydrogen malonate**; azure line: **1H hydrogen succinate**; blue line: **1H hydrogen fumarate**; green line: **1 HCl**).

Conclusions

In this study four lidocaine molecular salts of dicarboxylic acids in the form of hydrogen oxalate, hydrogen fumarate, hydrogen malonate and hydrogen succinate were synthesized and characterized by different solid-state techniques. SS NMR characterization allowed the distinction between molecular salts and co-crystals to be made through the analysis of ^{13}C and ^{15}N shifts upon proton transfer from carboxylic to amine groups. All compounds can be described as salts either obtained by solid-state or solvent assisted methods. The hydrogen oxalate, hydrogen fumarate and hydrogen malonate salts were also characterized by single crystal XRD. The structure of the hydrogen succinate salt was obtained by combining powder diffracion and SS NMR data (Z' and ^{1}H-^{1}H and ^{1}H-^{13}C proximities observed in ^{1}H DQ CRAMPS and ^{1}H-^{13}C FSLG off-resonance HETCOR spectra) taking advantage of the structural similarity with the hydrogen fumarate salt. Advanced 2D SS NMR techniques provided useful insights on crystal packing and HB environments.
All molecular salts show an improvement of their physico-chemical stability with respect to both the free base and the hydroclhoryde. In fact, there is an important increasing of the melting points with respect to both free base and hydrochloride salt (up to about 120° and more). Furthermore, the dissolution tests of the salts obtained show a higher solubility in water in comparison to the free base, while, the values are lower than in the case of the hydrochloride salt solubility (about one order of magnitude). The solubility of an API is a very important feature which affects any further development of the drug long before undergoing pharmacological evaluation and other preclinical studies. However, one must keep in mind that making a drug molecule more water-soluble can also be a drawback. There is a general tendency that the more water-soluble a compound is, the more diffusible it is. This causes it to be less specific in its activity, and more liable to rapid elimination and, therefore, shorter acting.[18] In this sense, the co-crystal or salt formation can be seen as one of the best methods for tuning the physico-chemical properties of an API in order to find the good balance between solubility and dffusibility.

Acknowledgments

We acknowledge MIUR and the Universities of Bologna and Torino for financial support.

References

1 Lofgren, N. M.; Lundquist, B. J. *Alkyl Glycinalnilides. U.S. Patent 2 441 498,* May 11, 1948.

2 Fang-Yu Lee, Shan-Chiung Chen, Bin-Ken Chen, Chiung-Ju Tsai, Yen-Ling Yi, *US Patent 7 166 641 B2*, Jan. 23, 2007.

3 a) Gasparotti, Franca A., *US Patent 4 891 386*, Jan. 2, 1990; b) Fang-Yu Lee, Shan-Chiung Chen, Bin-Ken Chen, Chiung-Ju Tsai, Yen-Ling Yi, *US Patent 7 166 641 B2*, Jan. 23, 2007, c) Umeda Y., Nagase H., Makimura M., Tomono K., Shiro M., Ueda H., *Analytical Sciences*, 2007, **Vol.23**; d) Susan W. Larsen, JesperOstergaard, Sara V. Poulsen, Bjorn Schulz, Claus Larsen, *European Journal of Pharmaceutical Sciences*, 2007, **31**, 172-179; e) OpaVajragupta, Supreeya La-ong, *Drug Development and Industrial Pharmacy*, 1994, **20(17)**, 2671-2684; f) Y. Umeda, T. Fukami, T. Furuishi, T. Suzuki, K. Tanjoh, K. Tomono, Drug Development and Industrial Pharmacy, 2009, **35(7)**, 843-851.

4 a) S. L. James, C. J. Adams, C. Bolm, D. Braga, P. Collier, T. Friščić, F. Grepioni, K. D. M. Harris, G. Hyett, W. Jones, A. Krebs, J. Mack, L. Maini, A. G. Orpen, I. P. Parkin, W. C. Shearouse, J. W. Steed and D. C. Waddell, ***Chem. Soc. Rev.***, 2012, **41**, 413-447; b) S.Karki, T. Friscic and W. Jones, *CrystEngComm*, 2009, **11**, 470-481; c) D.R. Weyna, T. Shattock and M. J. Zaworotko, *Cryst. Growth Des.*, 2009, **9**, 1106-1123; d) M. J. Zaworotko, *Cryst. Growth Des..*, 2007, **7(4)**, 616-617; e) D. Braga, G. Palladino, M. Polito, K. Rubini, F. Grepioni, M.R. Chierotti and R. Gobetto, *Chem.-Eur. J.*, 2008, **14**, 1049-10159; f) D. Braga, F. Grepioni and M. T. Duarte, *Cryst. Growth Des.*, 2009, **9**, 5108-5116; g) T. Frisic and W. Jones, *Cryst. Growth Des.*, 2009, **9**, 1621-1637; h) G. Kaupp, *CrystEngComm*, 2009, **11**, 388-403; i) D. Braga, M. Curzi, E. Dichiarante, S.L. Giaffreda, F. Grepioni, L. Maini, G. Palladino, A. Pettersen, M. Polito, in *Making crystals from crystals: a solid-state route to the engineering of crystalline materials, polymorphs, solvates and co-crystals; considerations on the future of crystal engineering*, ed. L. Addadi, D. Braga and J.J. Novoa, Springer, The Netherlands, 2008, pp.131-156; j) M. R. Chierotti, L. Ferrero, N. Garino, R. Gobetto, L. Pellegrino, D. Braga, F. Grepioni and L. Maini, *Chem. Eur. J.*, 2010, **16**, 4347-4358.

5 D. Braga, L. Maini, C. Fagnano, P. Taddei, M.R. Chierotti, R. Gobetto, *Chem. Eur. J.* **2007**, 13, 1222-1230.)

6 (a) M.R. Chierotti, R. Gobetto, *Chem. Commun.* **2008**, 1621-1634; (b) S.P. Brown, *Macromol. Rapid Commun.* **2009**, 30, 688-716; (c) S.P. Brown, *Solid State Nucl. Magnetic Reson.* **2012**, 41, 1-27.

7 (a) R.K. Harris, *Solid State Sci.* **2004**, 6, 1025-1037; b) M.U. Schmidt, J. Bruning, J. Glinnemann, M.W. Hutzler, P. Morschel, S.N. Ivashevskaya, J. van de Streek, D. Braga, L. Maini, M.R. Chierotti, R. Gobetto, *Angew. Chem. Int. Ed.* **2011**, 50, 7924-7926.)

8 a) G. M. Sheldrick, *SHELX97, Program for Crystal Structure Determination*; University of Göttingen: Göttingen, Germany, 1997; b) C. F. Macrae, I. J. Bruno, J. A. Chisholm, P. R. Edgington, P. McCabe, E. Pidcock, L. Rodriguez-Monge, R. Taylor, J. van de Streek, P. A.

J. Wood, *Appl. Crystallogr*., 2008, **41**, 466−470; c) E. Keller, SCHAKAL99, Graphical Representation of Molecular Models, University of Freiburg, Germany, 1999; d) A. L. Speck, PLATON; *Acta Crystallogr*., *Sect*. *A*, 1990, **46**, C34.

9 A.C. Larson and R.B. Von Dreele, *"General Structure Analysis System (GSAS)"*, Los Alamos National Laboratory Report LAUR 86-748, 2000.

10 B.-J. van Rossum, C. P. de Groot, V. Ladizhansky, S. Vega, H. J. M. d. Groot, *J. Am. Chem. Soc.* **2000**, 122, 3465-3472.

11 R. Bettini, R. Menabeni, R. Tozzi, M.B. Pranzo, I. Pasquali, M.R. Chierotti, R. Gobetto, L. Pellegrino, *J. Pharm. Sci.* **2010**, 99, 1855-1870.

12 (a) E. Vinogradov, P.K. Madhu, S. Vega, *Chem. Phys. Lett.* 1999, **314**, 443-450; (b) M. Hohwy, H.J. Jakobsen, M. Edén, M.H. Levitt, N.C. Nielsen, *J. Chem. Phys.* 1998, **108**, 2686-2694.

13 a) P. Gilli and G. Gilli, in *Supramolecular Chemistry – From Molecules to Nanomaterials* (Vol. 6), Ed.s P. A. Gale and J. Steed, Wiley, Chichester, UK, 2012, pp. 2829-2867; b) D. Wiechert and D. Mootz, *Angew. Chem. Int. Ed.*, 1999, **38**, 1974-1976.

14 a) Z. Gu, A. McDermott, *J. Am. Chem. Soc.*, 1993, **115**, 4282; b) A. Naito, S. Ganapathy, K. Akasaka, C. J. McDowell, *J. Chem. Phys.*, 1981, **74**, 3198; c) D. Braga, L. Maini, G. De Sanctis, K. Rubini, F. Grepioni, M. R. Chierotti, R. Gobetto, *Chem. Eur. J*., 2003, **9**, 5538; d) R. Gobetto, C. Nervi, E. Valfrè, M. R. Chierotti, D. Braga, L. Maini, F. Grepioni, R. K. Harris, P. Y. Ghi, *Chem. Mater*., 2005, **17**, 1457; e) R. O. Duthaler, J. D. Roberts, *J. Magn. Reson.*, 1979, **34**, 129; f) R. E. Botto, J. D. Roberts, *J. Org. Chem.*, 1977, **42**, 2247.

15 a) E. Diez-Pena, I. Quijada-Garrido, J. M. Barrales-Rienda, I. Schnell, H.W. Spiess, *Macromol. Chem. Phys*., 2004, **205**, 430; b) D. Braga, F. Grepioni, M. Polito, M. R. Chierotti, S. Ellena, R. Gobetto, *Organometallics*, 2006, **25**, 4627; c) R. Gobetto, C. Nervi, M. R. Chierotti, D. Braga, L. Maini, F. Grepioni, R. K. Harris, P. Hodgkinson, *Chem. Eur. J*., 2005, **11**, 7461.

16 M. R. Chierotti, R. Gobetto, Chem. Commun. 2008, 1621-1634.

17 D. Braga, L. Maini, G. de Sanctis, K. Rubini, F. Grepioni, M. R. Chierotti, R. Gobetto, Chem. Eur. J. 2003, 9, 5538; d) R. Gobetto, C. Nervi, E. Valfrè, M. R. Chierotti, D. Braga, L. Maini, F. Grepioni, R. K. Harris, P. Y. Ghi, Chem. Mater. 2005, 17, 1457; e) R. O. Duthaler, J. D. Roberts, J. Magn. Reson. 1979, 34, 129.

18 C. G. Wermuth, P. H. Stahl, *Introduction*. in *Handbook of Pharmaceutical Salts: Properties, Selection, and Use*; P. H. Stahl, C. G. Wermuth , Eds.; VHCA and Wiley-VCH: Weinheim, 2002.